Massloss from viscous advective disc

Indranil Chattopadhyay *

Department of Astronomy and Space Science, Chungnam National Univ, Daejeon, South Korea

Santabrata Das

ARCSEC, Sejong University, Seoul, South Korea

Abstract

Rotating transonic flows are long known to admit standing or oscillating shocks and that the excess thermal energy in the post shock flow drives a part of the infalling matter as bipolar outflows. We compute massloss from a viscous advective disc. We show that the mass outflow rate decreases with increasing viscosity of the accretion disc, since viscosity weakens the centrifugal barrier that generates the shock. We also show that the optical depth of the post-shock matter decreases due to massloss which may soften the spectrum from such a mass losing disc.

Key words:
black hole physics, accretion, accretion discs, ISM: jets and outflows

1 Introduction

Accretion onto black holes has been intensely studied for the last three decades or so, to explain observed luminosities of galactic black hole candidates and AGNs, to explain their spectral states, and to explain the formation of jets or outflows etc. The formation of jets or outflows has been much debated about, because black holes do not have hard inner surface, from which infalling matter can bounce back to form outflows. Moreover, unlike stars there is no intrinsic atmosphere around black holes, from which outflows may originate. Lack of star-like atmosphere and non-existence of hard boundary, resulted

* Corresponding author.
Email addresses: indra@canopus.cnu.ac.kr (Indranil Chattopadhyay), sbdas@canopus.cnu.ac.kr (Santabrata Das).

in the general consensus that jets are formed from the accreting material itself. Therefore, the physics of accretion process is very very important to understand the mechanism which produces outflows. Moreover, Gallo *et al.* (2003), showed that jets originate from accretion discs which are in the hard spectral states ('hard states' are spectral states where the most power is in the high energy power-law end of the black hole spectrum). This suggests that the origin of jet is strongly correlated with state of accretion disc from which high energy emission dominates.

The unique inner boundary condition of black holes, sets it apart from the rest of the compact objects, *i.e.,* it has no hard surface and matter crosses the horizon with the speed of light (c). Therefore, at the horizon a black hole accretion is supersonic. Far off, the inflowing matter should be subsonic, hence black hole accretion is necessarily transonic. Liang & Thompson (1980), showed that transonic accretion solutions of rotating matter admit two X-type critical points. It was also shown that such transonic matter may enter through the outer critical point to become supersonic, suffers centrifugal pressure mediated shock, jumps to the higher entropy subsonic branch, and falls onto the black hole through the inner sonic point (Chakrabarti, 1989). Infact, theoretically there were two shock locations found. The non-uniqueness was removed by performing numerical simulations (Chakrabarti & Molteni, 1993), which showed the inner shock solution was dynamically unstable, while the outer one was stable.

Such a shocked accretion disc-model was used to compute the spectral states of the black hole candidates (Chakrabarti & Titarchuk, 1995; Chakrabarti *et al.* , 1996; Chattopadhyay *et al.* , 2003; Mandal & Chakrabarti, 2005; Chakrabarti & Mandal, 2006), where the post-shock tori — CENBOL (CENtrifugal Pressure supported BOundary Layer), produces the hard power-law tail by inverse-Comptonizing the softer photons from the outer disc.

Further studies of shocked accretion flow onto a black hole resulted in more interesting possibilities. Molteni *et al.* (1994), showed that for two dimensional accretion flow, significant turbulence is generated in the post-shock disc, which drives a significant portion of the inflowing matter as bipolar outflows. Molteni *et al.* (1996a), reconfirmed outflow formation when two-dimensional accretion flows were studied by two independent codes, namely with Smooth Particle Hydrodynamic code (SPH) and Total Variation Diminishing code (TVD). Moreover, these authors showed that generally the outflow is ejected between two geometric surfaces called the funnel wall (FW) and centrifugal barrier (CB). The details of these surfaces will be discussed bellow. In some cases, these authors computed mass outflow rates to be 10-15% of the accretion rate. The possibility of these outflows to be the precursor of relativistic jets, induced more theoretical investigations. Chakrabarti (1999), using a very simple inflow-outflow model, showed that these outflows are quenched

if shocks do not form. Moreover, Das *et al.* (2001a) showed that the outflow indeed decreases as the spectral state of the disc changes from hard to soft state. Several authors also reported that shocks may undergo oscillations either radially, or vertically or non-axisymmetrically (Molteni *et al.* , 1996b, 1999, 2001; Gu & Foglizzo, 2003), which may be interpreted as the cause for quasi periodic oscillations in hard photons. These oscillations will produce variable mass outflow rates, an area of further study, which has not yet been investigated thoroughly. Though these thermally driven outflows are not intrinsically relativistic (albeit transonic), introduction of radiative interactions from the disc to the outflows produced relativistic and collimated jets (Chattopadhyay & Chakrabarti, 2002; Chattopadhyay *et al.* , 2004; Chattopadhyay , 2005) from the post-shock CENBOL.

Most of the investigations listed above, on shocks in accretion disc and its consequences, have been done in the viscosity free limit. The issue of viscosity was studied at length mostly in subsonic discs (*e.g.,* Keplerian thin discs), with a viscosity prescription suitable for subsonic or insignificant radial inflow. Moreover, using Sakura-Sunyaev viscosity (Shakura & Sunyaev , 1973) prescription in flows which harbour discontinuities like shocks, the angular momentum distribution do not remain conserved even across a non-dissipative shock. A new prescription of viscosity was formulated (Chakrabarti & Molteni, 1995) for flows with significant radial velocity, such that the angular momentum distribution remains conserved across the shock. With such viscosity prescription, Chakrabarti (1996) presented the global solutions of the viscous flow. A more detailed study of such viscous flow was done by Chakrabarti & Das (2004), in which all possible solutions were presented, including a detailed study of the parameter space. However, observational consequences of such viscous flow has not been studied as yet. Neither the effect of viscosity on generating mass outflow have been studied. We know from earlier studies of inviscid advective discs, that the centrifugal barrier may introduce a shock wave in an advective disc, generating hot post shock flow. Moreover, the unbalanced thermal pressure drives a part of the matter as bipolar outflows (Chakrabarti, 1999). These outflows are basically thermally driven however they also depend on the angular momentum of the disc. Thus it is generally found that with increasing energy and/or increasing angular momentum of the flow, mass outflow rates are enhanced. It is to be remembered that, as viscous flow approaches the black hole, angular momentum decreases while energy increases. Thus there are two competing processes to determine the shock location, as we increase the viscosity. Should the shock move inwards as we increase the viscosity for flows with identical outer boundary conditions or vice-versa? How would the position of shock affect the mass outflow rates? As far as we are aware, till todate there is no theoretical attempt to compute mass outflow rates from a viscous advective disc. In the present paper we attempt to study the effect of viscosity on massloss, in particular, we will address the issue of shock dynamics and consequently on outflow generation. Furthermore, Lanzafame *et al.*

(1998), commented that simulations of viscous transonic flows show that the mass outflow rate may decrease with increasing viscosity, though it was not explicitly shown. We want to check whether this is true and if so, why.

In the next section, we present the model assumptions and the equations of motion of the disc-jet system. In §3, we present the results, and in the last section we draw concluding remarks.

2 Model Assumptions and Equations of motion

We begin with a steady, thin, viscous, axisymmetric accretion flow on to a Schwarzschild black hole. The space-time geometry around a Schwarzschild black hole is dictated by the pseudo-Newtonian potential introduced by Paczyński & Wiita (PW80) to avoid complexity. The expression for the pseudo-Newtonian potential is given by,

$$g(r) = -\frac{GM_{\rm BH}}{\left[r - \frac{2GM_{\rm BH}}{c^2}\right]},$$

where, G, $M_{\rm BH}$, and c are the gravitational constant, the mass of the black hole, and the velocity of light, respectively.

In Fig. 1, a schematic cartoon diagram of an advective accretion disc is presented. In this figure the pre-shock flow, the shock location (x_s), the post-shock flow (abbreviated as CENBOL) and the jet between the funnel wall (FW) and centrifugal barrier (CB) have been marked (we define FW and CB in §2.3.1). The figure is presented with up-down symmetry, however axisymmetry is also assumed.

We use a system of units where, $2G = M_{\rm BH} = c = 1$. In the steady state, the dimensionless hydrodynamic equations that govern the motion of infalling matter are (Chakrabarti, 1996),

(a) the radial momentum equation :

$$u\frac{du}{dx} + \frac{1}{\rho}\frac{dP}{dx} - \frac{\lambda^2(x)}{x^3} + \frac{1}{2(x-1)^2} = 0, \qquad (1a)$$

(b) the baryon number conservation equation :

$$\dot{M} = 2\pi\Sigma u x, \qquad (1b)$$

(c) the angular momentum conservation equation :

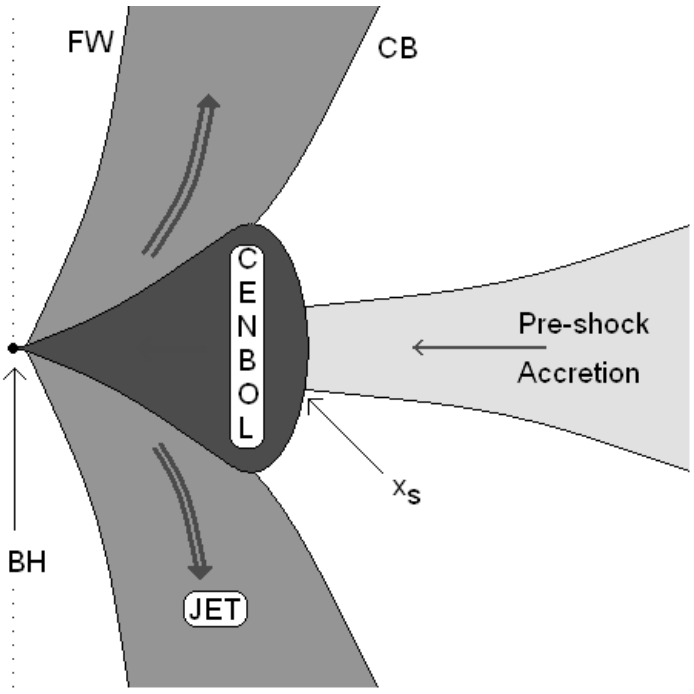

Fig. 1. Schematic diagram of disc-jet system with the position of black hole (BH), shock location (x_s), CENBOL, centrifugal barrier (CB), funnel wall (FW) etc are shown. The figure is shown with updown symmetry. The dotted line is the axis of symmetry and the equatorial plane (not shown) is a line perpendicular to the axis and passing through the black hole location dividing the system in two equal halves.

$$u\frac{d\lambda(x)}{dx} + \frac{1}{\Sigma x}\frac{d}{dx}\left(x^2 W_{x\phi}\right) = 0, \tag{1c}$$

and finally,

(d) the entropy generation equation :

$$\Sigma u T \frac{ds}{dx} = Q^+ - Q^-, \tag{1d}$$

where, flow variables u, ρ, P and $\lambda(x)$ in the above equations are the radial velocity, density, isotropic pressure and specific angular momentum of the flow respectively. Here Σ and $W_{x\phi}$ denote the vertically integrated density (Matsumoto *et al.* , 1984) and the viscous stress, s is the specific entropy of the flow, T is the local temperature. Q^+ and Q^- are the heat gained and lost by the flow (integrated in the vertical direction) respectively.

The present model is constructed in such a way that the disk is assumed to be in hydrostatic equilibrium in the vertical direction and therefore, local disk

height is obtained as,

$$h = \sqrt{\frac{2}{\gamma}} a x^{1/2} (x - 1). \tag{2}$$

Here, a is the adiabatic sound speed defined as $a = \sqrt{\gamma P/\rho}$, and $\gamma (= 4/3)$ is the adiabatic index. We shall use the Chakrabarti's viscosity prescription (Chakrabarti, 1996) which is valid for flows with significant radial motion. Since accretion flow possesses substantial amount of angular momentum, flow must be centrifugally supported and the knowledge of angular momentum distribution is important. The viscous stress is given by (Chakrabarti & Molteni, 1995; Chakrabarti, 1996),

$$W_{x\phi} = -\alpha_{\Pi} \Pi, \tag{3}$$

where, Π is the total pressure (thermal+ram) of the flow. This viscosity prescription ensures that the viscous stress is continuous across the axisymmetric shock wave. It is to be noted that, viscosity not only transport angular momentum, it also heat up the gas. Therefore, viscosity which appears in Eqs. (1c) and (1d), will generate heat as well as, transport angular momentum. To study the effect of angular momentum transport and heating properly, we ignore all types of cooling mechanisms in the present paper.

2.1 Sonic Point Analysis

At the outer edge of the disc, matter is subsonic, while on the horizon it is supersonic. Therefore, black hole accretion is necessarily transonic, *i.e.,* the flow velocity should match the local sound speed at one or more regions between the outer edge and the horizon, and such special regions are called critical points or sonic points (Chakrabarti, 1990).

We further simplify Eq. (1d),

$$\frac{u}{\gamma - 1} \left[\frac{1}{\rho} \frac{dP}{dx} - \frac{\gamma P}{\rho^2} \frac{d\rho}{dx} \right] = -H, \tag{4}$$

where, the heating term $H (= Q^+/\rho h)$ is given by,

$$H = Ax(ga^2 + \gamma u^2) \frac{d\Omega}{dx}. \tag{5}$$

In Eq. (5), $A = -\alpha_{\Pi} I_n/\gamma$, $g = I_{n+1}/I_n$, $n = 1/(\gamma - 1)$, $I_n = (2^n n!)^2/(2n + 1)!$ (Matsumoto *et al.* , 1984), and $\Omega(x)$ is the local angular velocity of the flow.

Equations (1a-1c), and (4), can be combined and we get a first-order linear differential equation,

$$\frac{du}{dx} = \frac{N}{D}, \tag{6}$$

where,

$$N = -\frac{\alpha_\Pi A(ga^2+\gamma u^2)^2}{\gamma x} - \left[\frac{\lambda^2}{x^3} - \frac{1}{2(x-1)^2}\right]\left[2\alpha_\Pi g A(ga^2+\gamma u^2) + \frac{(\gamma+1)u^2}{(\gamma-1)}\right]$$
$$- \frac{u^2a^2(5x-3)}{x(\gamma-1)(x-1)} - \frac{(ga^2+\gamma u^2)}{x}\left[\frac{\alpha_\Pi g A a^2(5x-3)}{\gamma(x-1)} - \frac{2\lambda A u}{x}\right], \tag{7}$$

and,

$$D = \frac{2a^2u}{\gamma-1} - \frac{(\gamma+1)u^3}{(\gamma-1)} - A\alpha_\Pi u(ga^2+\gamma u^2)\left[(2g-1) - \frac{a^2 g}{\gamma u^2}\right] \tag{8}$$

At the sonic point (x_c), both N and D must vanish simultaneously. At x_c, from Eq. (8), we get the expression for Mach number ($M = u/a$) at x_c,

$$M(x_c) = \sqrt{\frac{-m_b - \sqrt{m_b^2 - 4m_a m_c}}{2m_a}}, \tag{9}$$

where,

$$m_a = -A\alpha_\Pi\gamma^2(\gamma-1)(2g-1) - \gamma(\gamma+1),$$
$$m_b = 2\gamma - 2A\alpha_\Pi g\gamma(\gamma-1)(g-1),$$

and

$$m_c = A\alpha_\Pi\gamma^2(\gamma-1).$$

Similarly at x_c, Eq. (7) yields,

$$\left[\frac{\alpha_\Pi A(g+\gamma M^2)^2}{\gamma x_c} + \frac{\alpha_\Pi A(5x_c-3)(g+\gamma M^2)}{\gamma x_c(x_c-1)} + \frac{M^2(5x_c-3)}{x_c(\gamma-1)(x_c-1)}\right]a_c^2$$
$$- \frac{2\lambda A M(g+\gamma M^2)}{x_c^2}a_c + \left[\frac{\lambda^2}{x_c^3} - \frac{1}{2(x_c-1)^2}\right]$$
$$\times\left[2\alpha_\Pi g A(g+\gamma M^2) + \frac{(\gamma+1)M^2}{(\gamma-1)}\right] = 0. \tag{10}$$

The gradient of velocity [Eq. (6)] at the sonic point is determined by L'Hospital rule. It has been shown that such flows may posses at most three sonic points between the outer edge and the horizon (Das *et al.* , 2001b) out of which, two (outer x_{co} and inner x_{ci} sonic points) are saddle type and the middle one (x_{mid}) is spiral type (or O type for inviscid flow). The necessary condition

to form shocks in a black hole accretion is the simultaneous existence of x_{ci} and x_{co}. In inviscid flow, if the specific energy ($\mathcal{E}$) and λ is specified then the entire set of global solutions can be uniquely determined. However, in presence of dissipation both $\mathcal{E}$ and λ may vary, which makes solving Eqs. (1a-1d) more complicated. To solve these equations we supply x_{ci}, the specific angular momentum λ_i (at x_{ci}) and α_Π, and integrate inward and outward. The entire class of solutions have been presented in Chakrabarti & Das (2004), interested reader may go through them. In the present paper, we are interested to compute the mass outflow rates from the viscous accretion disc.

2.2 Shock Conditions

In absence of massloss, the Rankine-Hugoniot shock conditions are given by,

(a) the energy flux is continuous across the shock —

$$\mathcal{E}_+ = \mathcal{E}_-, \tag{11a}$$

(b) the mass flux is continuous across the shock —

$$\dot{M}_+ = \dot{M}_-, \tag{11b}$$

and finally, (c) the momentum balance condition —

$$W_+ + \Sigma_+ u^2{}_+ = W_- + \Sigma_- u_-^2, \tag{11c}$$

where W is the vertically integrated thermal pressure and subscripts "$-$" and "$+$" refer, respectively, to quantities before and after the shock.

In presence of mass outflow, Eq. (11b) is to be modified,

$$\dot{M}_+ = \dot{M}_- - \dot{M}_{\rm out} = \dot{M}_-(1 - R_{\dot{m}}), \tag{11d}$$

where $R_{\dot{m}} = \dot{M}_{\rm out}/\dot{M}_-$ is the ratio between mass flux of the outflow and the pre-shock accretion rate (accretion rate through x_{co}).

The l. h. s of Eq. (11c) is given by,

$$W_+ + \Sigma_+ u^2{}_+ = \frac{2I_n\dot{M}_+}{\gamma 4\pi x_s v_+}(g a_+^2 + \gamma v_+^2) = \frac{2I_n\dot{M}_+\Theta_+}{\gamma 4\pi x_s v_+}, \tag{12a}$$

where, x_s is the shock location. From Eqs. (11c-11d) the pre-shock sound speed can be expressed as,

$$a_-^2 = \frac{C_1 v_-}{g} - \frac{\gamma v_-^2}{g}, \tag{12b}$$

where $C_1 = (1 - R_{\dot{m}})\Theta_+/v_+$. And from Eq. (11a), we have,

$$\left[1 - \frac{2\gamma}{g(\gamma-1)}\right] v_-^2 + \frac{2C_1}{g(\gamma-1)} v_- + \left[\frac{\lambda^2}{x_s^2} - \frac{1}{x_s - 1} - 2\mathcal{E}_+\right] = 0 \qquad (12c)$$

The procedure to find shock is, to use Eqs. (12b-12c) to compute supersonic branch quantities, from post-shock subsonic branch local quantities. These supersonic branch quantities are then used to find x_{co}. However, to find the shock one needs to know the mass-outflow rate too, *i.e.,* one needs to solve the outflow and accretion solution simultaneously. It is to be noted that Eqs. (12b-12c) was derived for no massloss case by Chakrabarti & Das (2004). The difference induced by massloss, is that the post-shock pressure decreases. Therefore the shock will move closer to gain the pressure balance condition (at the shock), if we allow massloss.

2.3 Self consistent computation of massloss

From numerical simulations by Molteni *et al.* (1996a) (Fig. 4a & 4b), we see that the outflowing matter tends to be in between two surfaces, the funnel wall (FW) and the centrifugal barrier (CB) surfaces. In Fig. 2, the schematic diagram of the jet geometry is shown. Geometric surfaces CB and FW are marked in the figure. The definitions of CB and FW are given bellow, and the jet coordinate $r_j(x_j, y_j)$ are also shown in the figure. We now describe the method by which we calculate the streamlines of the jet.

2.3.1 Jet Geometry

The centrifugal barrier (CB) surface is achieved from the pressure maxima condition:

$$\frac{\lambda^2}{x_{CB}^3} = \frac{x_{CB}}{2r_{CB}(r_{CB}-1)^2}, \qquad (13a)$$

where, $r_{CB}^2 = x_{CB}^2 + y_{CB}^2 \equiv$ spherical radius of CB. And x_{CB}, y_{CB} are the cylindrical radius and axial coordinate (or height at r_{CB}) of CB.

Simplifying Eq. (7a),

$$x_{CB} = \left[2\lambda^2 r_{CB}(r_{CB}-1)\right]^{1/4}, \qquad (13b)$$

and

$$y_{CB} = r_{CB}^2 - \lambda\sqrt{2r_{CB}}(r_{CB}-1). \qquad (13c)$$

Let,

$$y_{FW} = y_j = y_{CB}, \qquad (13d)$$

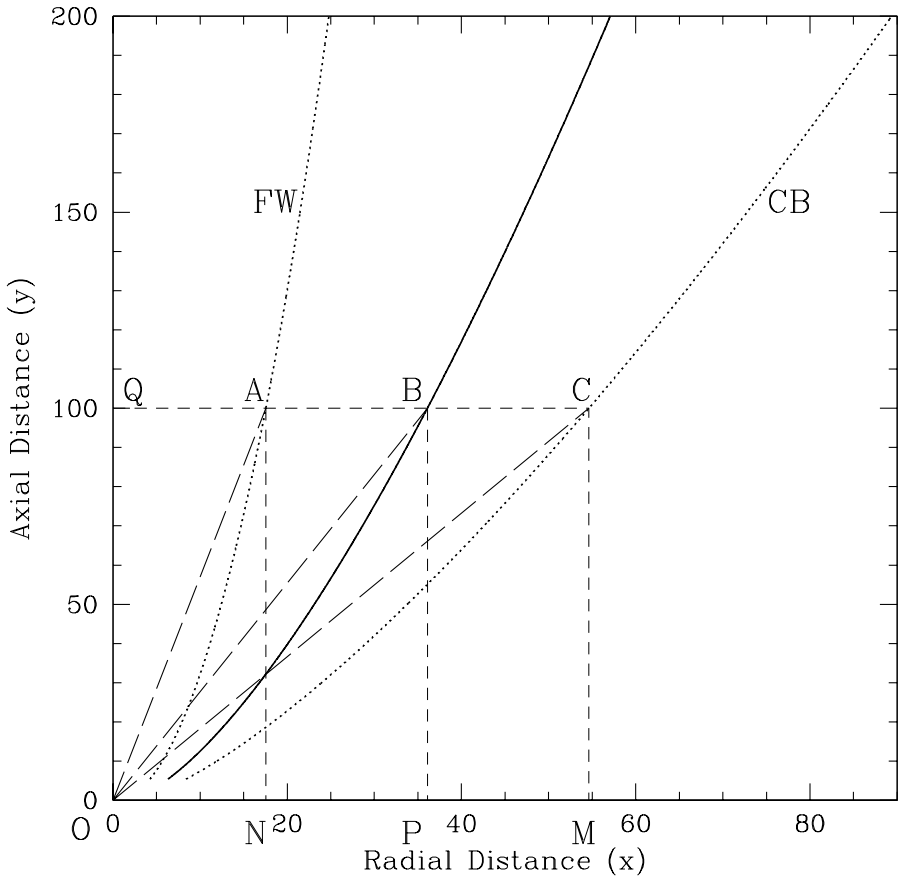

Fig. 2. Jet geometry for $\lambda = 1.75$. In figure $OA = r_{FW}$, $OC = r_{CB}$, $QC = x_{CB}$, $CM = y_{CB}$; $CM = BP(y_j) = AN(y_{FW})$; $QA = x_{FW}$; $QB = x_j$; And $OB = r_j = \sqrt{x_j^2 + y_j^2}$. FW and CB are marked in the figure.

where y_{FW} height of funnel wall (FW), and y_j height of the jet at r_{CB}.

The Funnel Wall (FW) is defined where the effective potential is zero,

$$\frac{\lambda^2}{x_{FW}^2} = \frac{1}{r_{FW} - 1}, \tag{13e}$$

where, $r_{FW}^2 = x_{FW}^2 + y_{FW}^2 \equiv$ spherical radius, and x_{FW} is the cylindrical radius of FW.

Simplifying Eq. (13e), with the help of Eq. (13d), we have,

$$x_{FW}^2 = \lambda^2 \frac{(\lambda^2 - 2) + \sqrt{(\lambda^2 - 2)^2 - 4(1 - y_{CB}^2)}}{2}, \tag{13f}$$

From Eqs. (13b) and (13f), we estimate the cylindrical radius of the outflow

$$x_j = \frac{x_{FW} + x_{CB}}{2}, \tag{13g}$$

From Eqs. (13c), (13d), (13g), we get the spherical radius of the jet.

$$r_j = \sqrt{x_j^2 + y_j^2}, \tag{13i}$$

In Fig. 2, $OB = r_j$, and defines the streamline of the outflow.

The total area function of the jet (about the equatorial plane), is given by,

$$\mathcal{A} = 2\pi(x_{CB}^2 - x_{FW}^2) \tag{13j}$$

2.3.2 Jet equations

We assume the jet to be inviscid. The jets are supposed to be lighter than accretion disc, and definitely of lower angular momentum, than atleast the outer edge of the disc. Consequently, the differential rotation should also be much less than in the accretion disc. There should be some cooling mechanism in jets, but since we disregard all types of cooling mechanism in this paper, we don't consider them for jets. Equation of motions for jet can be expressed as, the integrated momentum balance equation,

$$\mathcal{E}_j = \frac{1}{2}v_j^2 + na_j^2 + \frac{\lambda_j^2}{2x_j^2} - \frac{1}{2(r_j - 1)}, \tag{14a}$$

where $\mathcal{E}_j$ is the specific energy of the jet. The integrated continuity equation:

$$\dot{M}_{\rm out} = \rho_j v_j \mathcal{A}, \tag{14b}$$

and instead of the entropy generation equation we have the polytropic equation ($p_j = K_j \rho_j^\gamma$) of state for the jet. Moreover, the specific energy of the jet is the specific energy of the accretion disc at the shock *i.e.,* $\mathcal{E}_j = \mathcal{E}_s$, and the angular momentum of the jet should be the angular momentum of the accretion at the shock $\lambda_j = \lambda_s$. The polytropic index of the jet $[n = 1/(\gamma - 1)]$ is same as that of the accretion disc.

In Eqs. (14a-14b), the suffix 'j' indicates jet variables, where v_j, a_j, and ρ_j are the velocity, the sound speed and the density of the jet. The spatial coordinates r_j and x_j are the spherical radial coordinate and cylindrical radial coordinate of jet defined in Eqs. (13g-13i). All the derivatives are taken with respect to r_{CB}, since we have taken the CB surface as the reference surface of the jet, i.e., $r_j \equiv r_j(r_{CB})$. For simplicity we assign $r = r_{CB}$. All information of jet distance

will be obtained in terms of r (*i.e.,* $r_{\rm CB}$), and the jet coordinates are calculated by using Eqs. (13b-13i).

We differentiate Eqs. (14a) and (14b), eliminate da_j/dr, and get the expression for dv_j/dr. Following similar procedure as in §2.1, we find the sonic point conditions for jet/outflow which are given by,

$$a_{jc}^2 = \left[\frac{1}{2(r_{jc}-1)^2}\left(\frac{dr_j}{dr}\right)_{r_c} - \frac{\lambda^2}{x_{jc}^3}\left(\frac{dx_j}{dr}\right)_{r_c}\right]\left[\frac{1}{\mathcal{A}_c}\left(\frac{d\mathcal{A}}{dr}\right)_{r_c}\right]^{-1}, \tag{14c}$$

and

$$v_{jc}^2 = a_{jc}^2. \tag{14d}$$

Putting Eqs. (14c-14d) in Eq. (14a), one uniquely determines the sonic point (r_{jc}) of the jet as a function of $(\mathcal{E}_j, \lambda_j)$, which in turn determines a_{jc}. The derivatives at the jet sonic point are obtained by employing L'Hospital rule similar to the accretion disc case. Once the sonic point and the values of the necessary variables at the sonic is obtained, we integrate from sonic point inwards upto the shock in accretion. We assume $r = x_s$ as the jet base. We assume that the density of the jet at x_s is given by $\rho_j(x_s) = \rho_+$ (the post-shock density of the disc at x_s). The mass flux of the outflow is obtained by supplying the value of v_j, ρ_j and $\mathcal{A}$ of the jet at $r = x_s$ in Eq. (14b). To summarize, we assume that at the base, the outflows are being launched with the same energy, angular momentum and mass density of the immediate post-shock region of the accretion disc.

2.3.3 Inflow-Outflow solution

The expression for mass outflow rate is given by

$$R_{\dot{m}} = \frac{\dot{M}_{\rm out}}{\dot{M}_-} = \frac{\rho_j(x_s)v_j(x_s)\mathcal{A}(x_s)}{4\pi x_s h_- \rho_- u_-} = \frac{Rv_j(x_s)\mathcal{A}(x_s)}{4\pi x_s h_+ u_-} = \frac{Rv_j(x_s)\mathcal{A}(x_s)}{4\pi\sqrt{\frac{2}{\gamma}}x_s^{3/2}(x_s-1)a_+u_-}, \tag{15a}$$

where the compression ratio is given by,

$$R = \frac{\Sigma_+}{\Sigma_-} = \frac{\rho_+ h_+}{\rho_- h_-} \tag{15b}$$

The self-consistent method to find shocks in presence of the massloss is the following, initially the massloss is not considered, and the shock is found out for accretion flows, using the value of $(\mathcal{E}_s, \lambda_s)$ as inputs we solve for the outflow, and find the values of jet variables at x_s, and use Eq. (15a) to calculate $R_{\dot{m}}$,

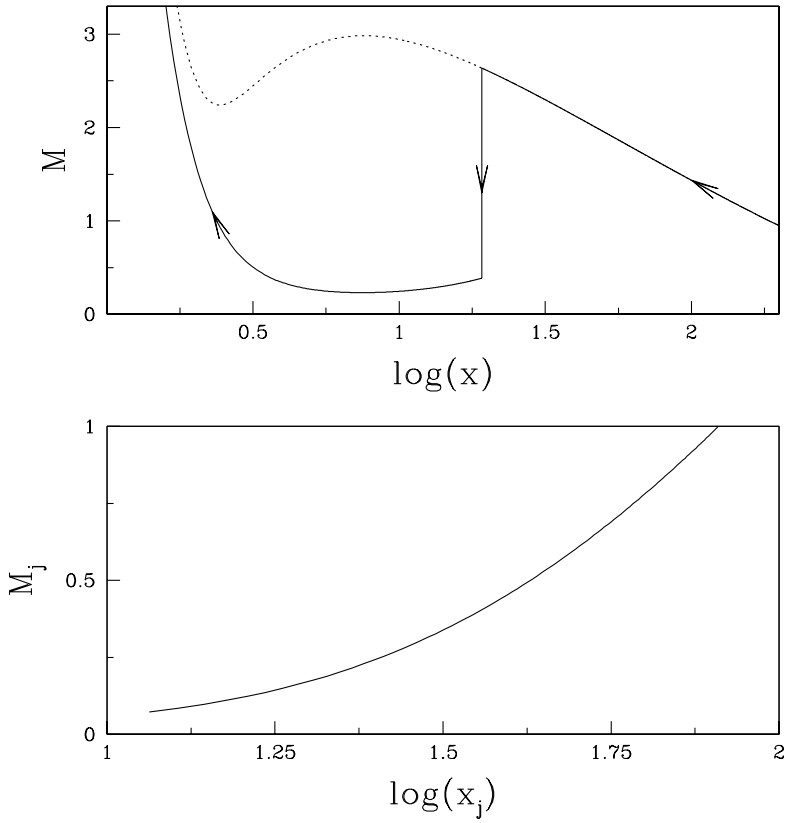

Fig. 3. Inflow-Outflow solution: Inflow Mach number M (upper panel) and that of outflow M_j (lower panel) with $log(x)$. The quantities for inflow are $x_{ci} = 2.445$, $\lambda_i = 1.75$, and $\alpha_\Pi = 0.002$, $x_s = 19.21$, $\mathcal{E}_s = 0.0014$, $\lambda_s = 1.756$ $x_{co} = 206.49$, $\lambda_o = 1.7716$. $R_{\dot{m}} = 0.055$, the outflow sonic point $x_{jc} = 81.2629$ ($r_{jc} = 346.1823$), and the jet coordinates at the base is given by $x_{jb} = 10.27$ ($r_{jb} = 16.62$).

supply this value in shock condition relations in Eqs. (12b-12c), and recalculate the shock location. We iterate this process till the solutions converge.

3 Results

In Fig. 3, the topology of inflow-outflow solution is presented. In the top panel the Mach number of the accretion flow is plotted with $log(x)$. The solid line marked with arrows present the accretion solution with the location of shock denoted by the vertical solid line with arrow. The dotted line shows the solution through which matter would have dived onto the black hole, had there been no shock. Inner sonic point and angular momentum are $x_{ci} = 2.445$, $\lambda_i = 1.75$, and the viscosity parameter is $\alpha_\Pi = 0.002$. The shock is at $x_s = 19.21$. The specific energy and angular momentum of the flow at the

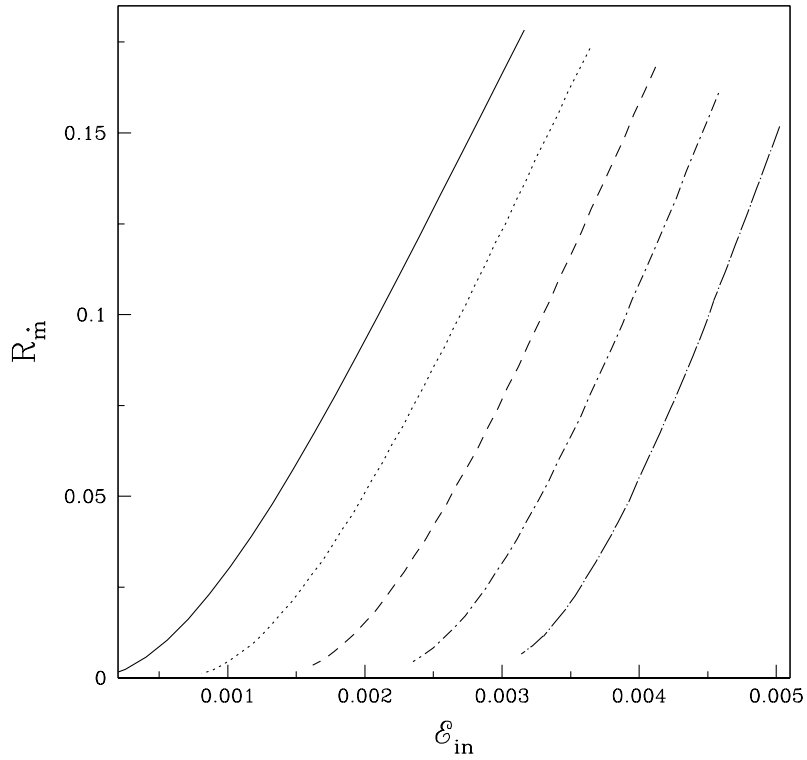

Fig. 4. Variation $R_{\dot{m}}$ with $\mathcal{E}_{\rm in}$, for $\alpha_\Pi = 0$ (solid), 0.005 (dotted), 0.01 (dashed), and 0.015 (dashed-dotted), 0.02 (long-dashed) respectively, and $\lambda_i = 1.75$.

shock are $\mathcal{E}_s = 0.0014$ and $\lambda_s = 1.756$, respectively. The outer sonic point is $x_{co} = 206.49$. In the lower panel, the Mach number of the outflow M_j is plotted with $log(x_j)$, where x_j is the cylindrical radius of the outflow. The outflow is plotted upto its sonic point ($x_{jc} = 81.2629$). The calculated mass outflow rate is $R_{\dot{m}} = 0.055$. It is to be noted that the, cylindrical radius of the jet at its base is $x_{jb} < x_s$, this is because at the jet base $r_{CB} = x_s$. The outflow solution is not plotted with the accretion solution since, these two has different flow geometry.

Let us now turn our attention on how viscosity affects shock formation and mass outflow rates. In Fig. 4, $R_{\dot{m}}$ is plotted with $\mathcal{E}_{\rm in}$ (the specific energy at x_{ci}), for $\alpha_\Pi = 0$ (solid), 0.005 (dotted), 0.01 (dashed), and 0.015 (dashed-dotted), and 0.02 (long dashed) respectively. The specific angular momentum at x_{ci} is kept fixed at $\lambda_i = 1.75$. This figure shows that $R_{\dot{m}}$ increases for more energetic flow. Interestingly, we see as α_Π is increased, $R_{\dot{m}}$ decreases, a fact reported in simulations (Lanzafame *et al.* , 1998). For the same value of $\mathcal{E}_{\rm in}$, if α_Π is increased by 0.005 then $R_{\dot{m}}$ is decreased by a factor of $\sim$2. However, if high

enough $\mathcal{E}_{\rm in}$ is chosen then one may get high $R_{\dot{m}}$ ($\gtrsim 10\%$).

In Fig. 5a, $R_{\dot{m}}$ is plotted with α_Π, for $\lambda_i = 1.8$ (solid), 1.775 (dashed) and 1.75 (dotted), respectively. The inner sonic points are $x_{ci} = 2.313$ (solid), 2.375 (dashed), 2.445 (dotted). The mass outflow rates increase with increasing angular momentum. It is also clearly shown that mass outflow rates decrease with increasing viscosity. The mass loss is less than 1% for $\alpha_\Pi \sim 0.01$, while $R_{\dot{m}} \gtrsim 10\%$ in the inviscid limit. In Fig. 5b, shock location (x_s) is plotted with α_Π, for solutions without massloss (dotted) and with massloss (solid). The parameters are same as the dotted curve of Fig. 5a, *i.e.,* $(\lambda_i, x_{ci}) = (1.75, 2.445)$, which we choose to be a representative case. It is to be remembered that the dotted curve is a typical solution from Chakrabarti & Das (2004). We clearly show that massloss from the post-shock region of the disc, causes the shock to move in (dotted curve is higher value than the solid one). However, as α_Π is increased the two curve tend to converge. Since $R_{\dot{m}}$ decreases with α_Π, the difference in shock location also diminishes.

The question however is, why $R_{\dot{m}}$ decreases with α_Π? In all the cases presented here, the λ_i is same, therefore with increasing α_Π, there is moderate increase of $\lambda(x)$ as we integrate outwards, however, the $\mathcal{E}(x)$ decreases sharply, which results in the decreased value of x_s. In Fig. 5c the value of angular momentum at the shock λ_s is plotted with α_Π. The fractional increase of λ_s is $\sim$1.1%. In Fig. 5d the value of specific energy at the shock $\mathcal{E}_s$ is plotted with α_Π. The fractional decrease of $\mathcal{E}_s$ is $\sim$8.2%. As x_s decreases, the base area $\mathcal{A}$ of the jet decreases. The base velocity ($v_j(x_s)$) of the jet should decrease too. However the compression ratio will increase. In Fig. 5e, $v_j\mathcal{A}$ (solid) and R (dotted) is plotted with α_Π. The quantity $v_j\mathcal{A}$ decreases by 90%, while R increases by mere 60%. From Eq. (15a), we see that in the denominator of the expression for $R_{\dot{m}}$, there is a term $x_s h_+ u_- \equiv x_s^{3/2}(x_s - 1)a_+ u_-$. In Fig. 5f, both the quantities $x_s^{3/2}(x_s - 1)$ (dashed) and $a_+ u_-$ (solid) is plotted with α_Π. The quantity $x_s^{3/2}(x_s - 1)$ decreases by 37% and $a_+ u_-$ (multiplied by a factor 5×10^4 in the figure) increases by 42%. The input parameters for the last four figures are same as that of Fig. 5b. We see that as x_s decreases, decrease of $v_j\mathcal{A}$ dominates all other quantities in Eq. (15a), and hence $R_{\dot{m}}$ decreases.

In Figs. 5(b-f), we have fixed the following set of parameters (λ_i, x_{ci}), and increased α_Π to see how viscosity affects shock and consequently on $R_{\dot{m}}$. If one increases α_Π for fixed (λ_i, x_{ci}), then $\mathcal{E}_{\rm in}$ will decrease anyway [see Fig. (1c) of Chakrabarti & Das 2004], hence $\mathcal{E}_s$ will be lower for higher α_Π. Therefore, we have studied less energetic accretion flows though we have increased the α_Π parameter, and saw that for such flows increasing viscosity parameter decreases the shock location and therefore the mass outflow rate. The question is, what happens to flows starting with same outer boundary conditions, as viscosity is increased?

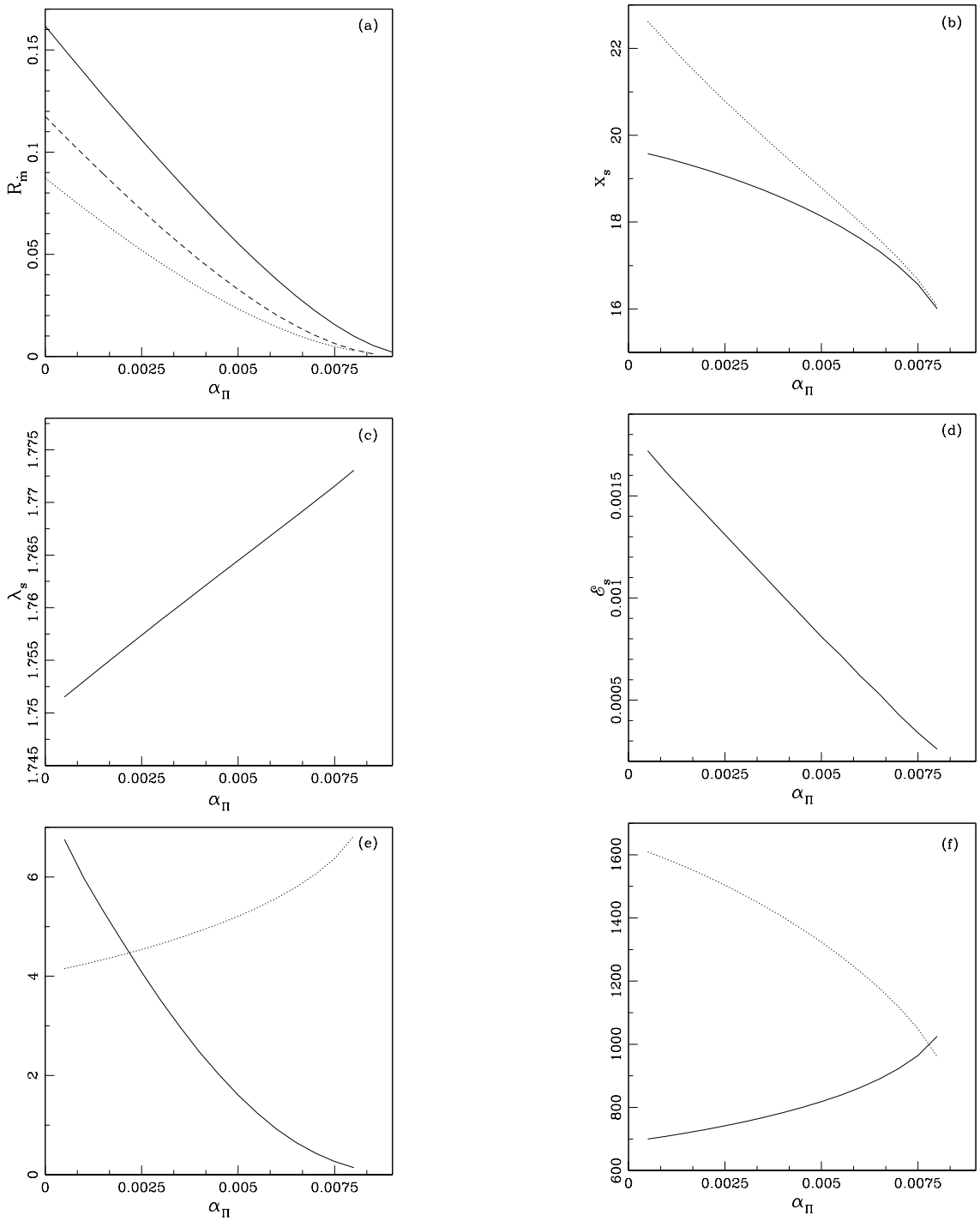

Fig. 5. (a) $R_{\dot{m}}$ vs α_Π, for for $\lambda_i = 1.8$ (solid), 1.775 (dashed) and 1.75 (dotted), respectively. Inner sonic points are $x_{ci} = 2.313$, 2.375, and 2.445, respectively. (b) Variation of x_s with α_Π, $\lambda_i = 1.75$ $x_{ci} = 2.445$. Dotted curve represents solution without massloss, and solid represents x_s with massloss. (c) Variation λ_s with α_Π,$\lambda_i = 1.75$ $x_{ci} = 2.445$. (d) Variation $\mathcal{E}_s$ with α_Π,$\lambda_i = 1.75$ $x_{ci} = 2.445$. (e) Variation of R (dotted) and $v_j\mathcal{A}$ (solid) with α_Π, $\lambda_i = 1.75$, $x_{ci} = 2.445$. (f) Variation of $x_s^{3/2}(x_s - 1)$ (dashed) and $a_{s+}u_- \times 5e + 4$ with α_Π, $\lambda_i = 1.75$, $x_{ci} = 2.445$.

In Fig. 6, we plot Mach number M (upper panel), λ (middle panel), and specific energy $\mathcal{E}$ (lower panel) with $log(x)$. The flow variables have been plotted for $\alpha_\Pi = 0$ (dashed) and $\alpha_\Pi = 0.003$ (dotted), and the flow variables have been launched with same energy and angular momentum $(\mathcal{E}_{\rm inj}, \lambda_{\rm inj}) = (0.002, 1.75)$ the outer edge being $x_{\rm inj} = 200$. Increasing α_Π decreases the shock location from $x_s = 20.3$ (dashed) to $x_s = 11.65$ (dotted), consequently mass outflow rate decreases from $R_{\dot{m}} = 0.093$ (dashed) to $R_{\dot{m}} = 0.07$. In this particular figure, we see that as viscosity is increased $\mathcal{E}(x)$ increases and $\lambda(x)$ decreases, but increase in $\mathcal{E}(x)$ cannot compensate the decrease in $\lambda(x)$, and hence the shock moves inwards. As shock moves inwards the jet area at the base decreases and mass out flow rate decreases. So in this particular case when the flow variables at the outer boundary has been kept fixed the position of the shock is determined mainly by the centrifugal force of the flow.

Therefore we may safely conclude that, if the outer boundary is fixed, then by increasing viscosity, the shock location and consequently the mass outflow rate is decreased.

Upto now, we have tried to show that the mass outflow rates strongly depends on shock location x_s, and formation of shocks itself depends crucially on the viscosity parameter. We have also shown that shocks are located closer to the black hole for viscous flows than in inviscid accretion flow. However, we are yet to comment on the observational consequence of such phenomena. Admittedly, it is beyond the scope of the present paper to compute the detailed spectrum of the flow, but we can make some qualitative remark on the spectral properties of such flows.

Chakrabarti & Titarchuk (1995) showed that hard power law photons were generated by inverse-Comptonization of soft photons from outer pre-shock region of the disc. They showed that excessive supply of soft photons compared to the shock heated electrons of the CENBOL cools down the post-shock disc and softens the spectrum.

Let us calculate the optical depth of the CENBOL, because this will help us to gain a qualitative understanding of the nature of the spectrum produced by the CENBOL. The definition of the optical depth for photons entering the CENBOL is given by,

$$\tau(x) = \int_{x_s}^{x} \kappa \rho dx',$$

where, κ is the opacity assuming Thompson scattering cross-section, and ρ is the density of the flow.

We consider the outer boundary condition of Fig. 6, *i.e.,* the outer edge is $x_{\rm inj} = 200$, the specific energy and angular momentum of the flow at $x_{\rm inj}$ are $(\mathcal{E}_{\rm inj}, \lambda_{\rm inj}) = (0.002, 1.75)$, for all the cases in Fig. 7. Moreover the mass accretion rate at $x_{\rm inj}$ is $\dot{M}_- = 0.3\dot{M}_{\rm Edd}$, and the central mass is $M_{BH} = 10 M_\odot$. In

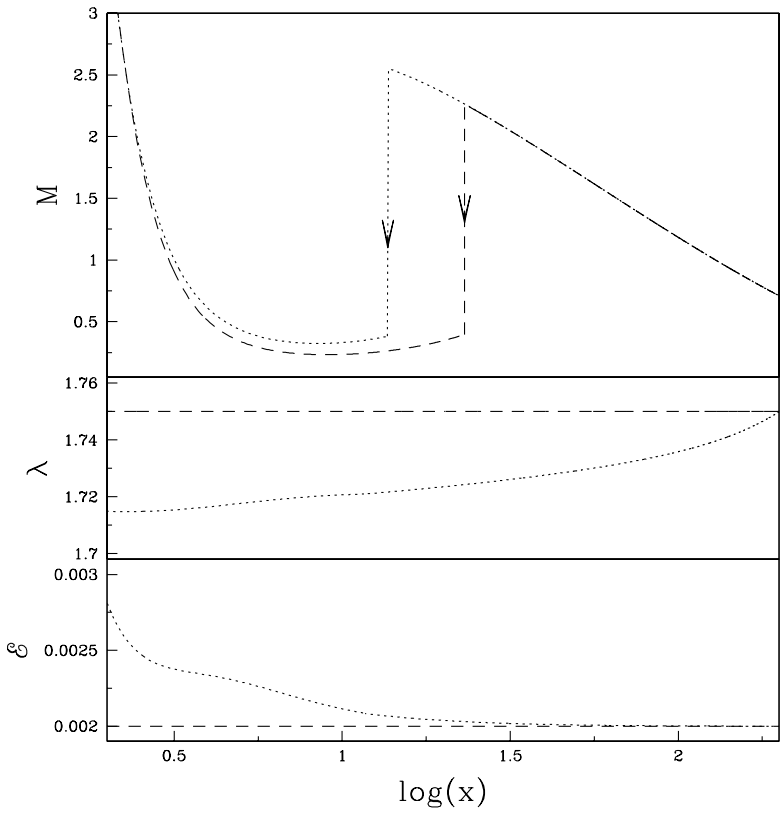

Fig. 6. Variation of M (upper panel), λ (middle panel), $\mathcal{E}$ (lower panel) with $log(x)$, for $\alpha_\Pi = 0$ (dashed) and $\alpha_\Pi = 0.003$ (dotted). The outer edge quantities are $x_{\rm inj} = 200$, $(\mathcal{E}_{\rm inj}, \lambda_{\rm inj}) = (0.002, 1.75)$. The shocks are $x_s = 20.3$ (dashed) and $x_s = 11.65$ (dotted).

Fig. 7, $\tau(x)$ is plotted only for the post-shock flow or the CENBOL, for the following viscosity parameter $\alpha_\Pi = 0$ with (dotted) and without (solid) considering massloss, and for $\alpha_\Pi = 0.003$ with (dashed-dotted) and without (dashed) massloss. Although all the solutions start with the same outer boundary, there are number of points to be noted from this figure. Even if we do not allow mass loss, shocks move closer in the viscous case (dashed) than the inviscid case (solid) from $x_s = 15$ to $x_s = 25$, respectively. Here, τ of the CENBOL is less for viscous case (dashed) compared to that of the non-viscous case (solid) since the path length decreases. For the massloss case, the shocks move closer to black hole in the viscous case (dashed-dotted) than the inviscid case (dotted). The massloss in the inviscid case (dotted) is about 12.4% so the shock moves inwards by quite a large distance. While in viscous case the massloss in about 9.3%, and hence the shock moves inwards by a lesser amount. However, if one compares τ between the viscous case with massloss (dashed-dotted) and with the inviscid no massloss case (solid), we see that the optical depth of the former is much lower. This is because viscosity and mass loss both decrease the

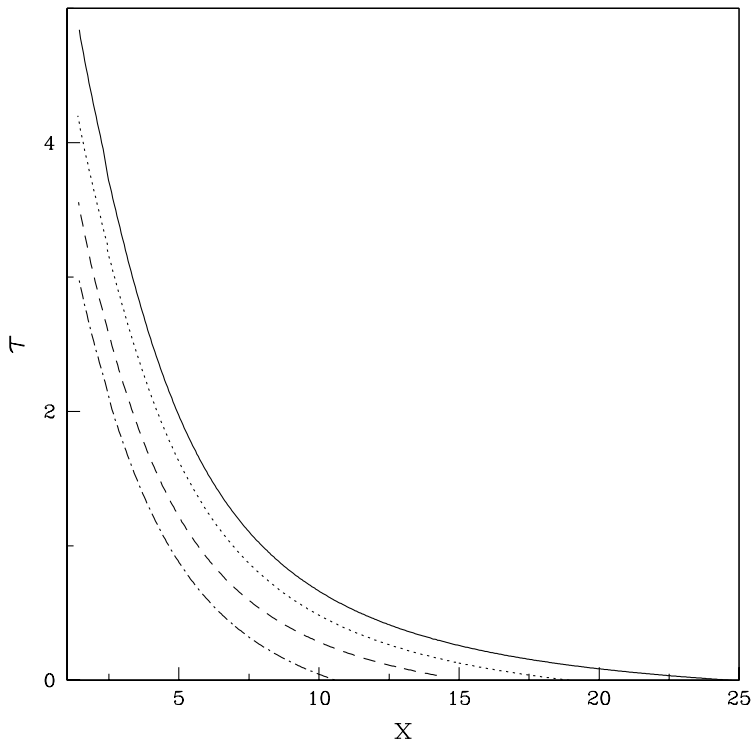

Fig. 7. Variation of τ with (x), for $(\alpha_\Pi, R_{\dot{m}}) = (0, 0)$ (solid), $(\alpha_\Pi, R_{\dot{m}}) = (0, 0.124)$ (dotted), $(\alpha_\Pi, R_{\dot{m}}) = (0.003, 0)$ (dashed), and $(\alpha_\Pi, R_{\dot{m}}) = (0.003, 0.099)$ (dashed-dotted). The outer edge quantities are $x_{\rm inj} = 200$, $(\mathcal{E}_{\rm inj}, \lambda_{\rm inj}) = (0.002, 1.75)$. Here τ is plotted for CENBOL.

value of x_s, moreover the density also gets reduced due to massloss and hence the τ for viscous flow with massloss decreases appreciably. This means more photons from the outer disc can penetrate the inner part of the CENBOL and there by cool it. A cooler CENBOL will evidently produce softer spectrum, than say in the inviscid case without massloss. Chakrabarti (1998), calculated spectrum of a disc which is loosing mass from post-shock region, and indeed he found that the spectrum softens. However, the shock location was supplied by hand, and viscosity was not considered. We predict that for realistic transonic flow solutions, the decrease of x_s due to the presence of massloss and viscosity, and decrease of density due to mass loss will soften the spectrum further. It seems that, if advective, transonic flow around black holes does exist, then the disc will enter in its 'hard' state as the disc is shocked. The hot post shock flow will emit outflows/jets because of excess thermal force along the vertical direction, however as the outflowing matter leaves the CENBOL, it will soften the emitted spectrum.

4 Concluding Remarks

The theory of transonic accretion flow has been studied extensively for around a couple of decades now. Early studies showed such flows may harbour standing or oscillating shocks (Chakrabarti, 1989). The presence of shocks were also thought to be the real cause behind hard state of the disc spectrum (Chakrabarti & Titarchuk, 1995), generating outflows (Chakrabarti, 1999) etc. Studies of shocks in viscous accretion disc were also undertaken, however as mentioned in §1, such efforts were confined to obtain the global solution for accretion flows with or without shocks and/or the detailed study of the parameter space (Chakrabarti, 1996; Chakrabarti & Das, 2004). Important as they are, since a proper understanding of them enhances the grasp on the physics of such flows, however no attempts have been undertaken to link these viscous flows with observables such as outflows and spectrum.

In this paper we have tried to improve our earlier computation of massloss (Das *et al.* , 2001a), by employing the knowledge of viscous disc solutions (Chakrabarti & Das, 2004). In the earlier paper the disc was considered to be inviscid and the jet was non-rotating. Furthermore, the shock condition was not modified for massloss. Presently we have included viscosity and considered rotating outflows, in particular we have concentrated on studying how viscosity affects shocks and in turn, how shocks affect the mass outflow rates.

We have shown that massloss from the post-shock disc reduces post-shock total pressure, and hence the shock front moves towards the black hole. We have also shown that the mass outflow rate depends on the energy of the flow as well as the angular momentum of the flow, and increasing both, in turn, increases the mass outflow rate.

However, less energetic accretion will produce lower mass outflow rates, even though angular momentum is increased outward, by increasing the viscosity parameter.

More interestingly, it has been shown that for matter starting with same outer boundary conditions, if viscosity is increased, mass outflow rate is decreased because the centrifugal barrier is weakened.

We have also shown that the post shock optical depth decreases in presence of viscosity and massloss, this should soften the spectrum emitted by such flow.

A detailed study of spectrum from such viscous discs, by including all possible cooling processes is under consideration and will be reported elsewhere.

Acknowledgements

IC was supported by the KOSEF grant R01-2004-000-10005-0, and SD was supported by KOSEF through Astrophysical Research Center for the Structure and Evolution of the Cosmos (ARCSEC).

References

Chakrabarti, S. K. 1989, ApJ 347, 365 (C89).
Chakrbarti, S. K. 1990, Theory of Transonic Astrophysical Flows, World Scientific Publishing, Singapore.
Chakrabarti, S. K., Molteni, D., 1993, ApJ, 417, 671.
Chakrabarti, S. K., Titarchuk, L., 1995, ApJ 455, 623.
Chakrabarti, S. K., Molteni, D., 1995, MNRAS, 272, 80.
Chakrabarti, S. K. 1996, ApJ, 464, 664.
Chakrabarti, S. K., Titarchuk, L., Kazanus, L., Ebisawa, K., 1996, A & AS 120, 163.
Chakrabarti, S. K., 1998, Ind. Journ. Phys. 72, 565.
Chakrabarti, S. K., 1999, A&A 351, 185.
Chakrabarti, S. K., Das, S., 2004, MNRAS, 349, 649.
Chakrabarti, S. K., Mandal, S., 2006, ApJL, 642, 49.
Chattopadhyay, I., Chakrabarti, S. K., 2002, MNRAS 333, 454.
Chattopadhyay, I., Das, S., Mandal, S., Chakrabarti, S. K., 2003, in Chakrabarti, S. K., Das, S., Basu, B.,Khan, M., eds, Proc. Recent Trends in Astro and Plasma Physics in India, CSP, Kolkata, p. 76.
Chattopadhyay, I., Das, S., Chakrabarti, S. K., 2004, MNRAS 348, 846.
Chattopadhyay, I., 2005, MNRAS 356, 145.
Das, S., Chattopadhyay, I., Nandi, A., Chakrabarti, S. K., 2001a, A&A 379, 683.
Das, S., Chattopadhyay, I., Chakrabarti, S. K., 2001b, ApJ 557, 983.
Gallo, E., Fender, R. P., Pooley, G. G., 2003, MNRAS, 344, 60.
Gu W. M., Foglizzo, T., 2003, A&A, 409, 1.
Lanzafame, G., Molteni, D., Chakrabarti, S. K., 1998, MNRAS, 299, 799.
Liang, E. P. T., Thompson, K. A., 1980, ApJ 240, 271L
Mandal, S., Chakrabarti, S. K., 2005, A&A, 434, 839.
Matsumoto, R, Kato, S., Fukue, J., Okazaki A. T., 1984, PASJ, 36, 71.
Molteni, D., Lanzafame, G., Chakrabarti, S. K., 1994, ApJ, 425, 161.
Molteni, D., Ryu, D., Chakrabarti, S. K., 1996, ApJ, 470, 460.
Molteni, D., Sponholtz, H., Chakrabarti, S. K., 1996, ApJ, 457, 805.
Molteni, D., Toth, G., Kuznetsov, O., 1999, ApJ, 516, 411.
Molteni, D., Acharyaa, K., Kuznetsov, O., Bisikalo, D., Chakrabarti, S. K., 2001, ApJL, 563, 57.

Shakura, N. I., Sunyaev, R. A., 1973, A& A 24, 337.